Available online at www.sciencedirect.com
SCIENCE DIRECT®
Journal of Magnetic Resonance 171 (2004) 233–243
JMR Journal of Magnetic Resonance
www.elsevier.com/locate/jmr

Communication

Modulation of the distance dependence of paramagnetic relaxation enhancements by CSA×DSA cross-correlation

Guido Pintacuda[a,b], Andrei Kaikkonen[b], Gottfried Otting[a,*]

[a] *Research School of Chemistry, Australian National University, Canberra, ACT 2605, Australia*
[b] *Department of Medical Biochemistry and Biophysics, Karolinska Institute, S-171 77 Stockholm, Sweden*

Received 11 June 2004; revised 25 August 2004
Available online 25 September 2004

Abstract

Paramagnetic metal ions with fast-relaxing electronic spin and anisotropic susceptibility tensor provide a rich source of structural information that can be derived from pseudo-contact shifts, residual dipolar couplings, dipole–dipole Curie spin cross-correlation, and paramagnetic relaxation enhancements. The present study draws attention to a cross-correlation effect between nuclear relaxation due to anisotropic chemical shielding (CSA) and due to the anisotropic dipolar shielding (DSA) caused by the electronic Curie spin. This CSA×DSA cross-correlation contribution seems to have been overlooked in previous interpretations of paramagnetic relaxation enhancements. It is shown to be sufficiently large to compromise the $1/r^6$ distance dependence usually assumed. The effect cannot experimentally be separated from auto-correlated DSA relaxation. It can increase or decrease the observed paramagnetic relaxation enhancement. Under certain conditions, the effect can dominate the entire paramagnetic relaxation, resulting in nuclear resonances narrower than in the absence of the paramagnetic center. CSA×DSA cross-correlation becomes important when paramagnetic relaxation is predominantly due to the Curie rather than the Solomon mechanism. Therefore the effect is most pronounced for relaxation by metal ions with large magnetic susceptibility and fast-relaxing electron spin. It most strongly affects paramagnetic enhancements of transverse relaxation in macromolecules and of longitudinal relaxation in small molecules.

1. Introduction

Enhanced relaxation of the nuclear spins surrounding a paramagnetic center constituted of one or several unpaired electrons presents one of the most obvious manifestations of paramagnetism [1]. The relaxation enhancement strongly depends on the distance between the nuclear and the electron spin. Since the effect can be observed for significantly longer distances than internuclear interactions, the measurement of paramagnetic relaxation enhancements (PRE) provides an attractive way of accessing long-range distance information between nuclear spins and paramagnetic centers. Consequently, paramagnetic compounds and metal ions have found wide-spread use as sources of long-range distance restraints for structure determination of molecules in solution [2,3], as indicators of stable or transient intermolecular contacts in molecular biology [4–8], enzymology [9], drug discovery [10–14], and organic catalytic synthesis [15–17], and as probes to study the binding of non-magnetic ions like magnesium or calcium to receptors [18–21]. In the presence of other, non-paramagnetic sources of nuclear relaxation, such as dipole–dipole and CSA relaxation, the net paramagnetic relaxation enhancement is usually determined as the difference in total relaxation rates between paramagnetic and diamagnetic molecules, i.e., in the presence and absence of the paramagnetic center.

* Corresponding author. Fax: +61 2 61250750.
E-mail address: gottfried.otting@anu.edu.au (G. Otting).

1090-7807/$ - see front matter © 2004 Elsevier Inc. All rights reserved.
doi:10.1016/j.jmr.2004.08.019

With regard to NMR studies in solution, paramagnetic centers fall into two different classes. Nitroxide radicals and metal ions like Cu^{2+}, Mn^{2+} or Gd^{3+} have an isotropic or, as in the case of Cu^{2+}, nearly isotropic magnetic susceptibility [22]. Combined with the absence of low-lying excited states, these paramagnetic centers are characterized by slowly relaxing electronic spins which affect the surrounding nuclear spins through a dipolar (''Solomon'') mechanism [23].

The second class comprises metal ions with fast-relaxing electron spins [22]. The fast modulation of the stochastic dipolar interaction between electron and nuclear spins results in smaller PRE effects for the nuclear spins. Such paramagnetic centers are thus more compatible with high-resolution NMR spectroscopy. In addition, they usually possess anisotropic magnetic susceptibilities which generate pseudocontact shifts and cause an alignment of the molecule with respect to the external magnetic field [24]. Efficient electronic relaxation combined with a large Zeeman splitting creates a net magnetic moment (Curie spin) in thermal equilibrium. Interaction of the Curie spin with nuclear spins constitutes an additional mechanism of nuclear relaxation [25,26]. It has been noted that the functional form of Curie-spin relaxation is analogous to that of CSA [27,28]. This similarity was further emphasized by Bertini et al. [29] who pointed out that the Curie contribution can be viewed as an effect originating from the anisotropy of the dipolar shielding (DSA) caused by the electronic susceptibility at the site of the nucleus.

The enhancement of longitudinal and transverse nuclear relaxation is inversely proportional to the sixth power of the proton–electron distance for both Solomon and Curie-spin relaxation mechanisms. Therefore, the simultaneous presence of both mechanisms presents no impediment to the measurement of experimental distances. Deconvolution of the individual contributions requires the accurate knowledge of the electronic and molecular correlation times [22].

Unlike Solomon relaxation which depends on the electronic spin relaxation, Curie relaxation like diamagnetic relaxation mechanisms is caused exclusively by the rotational reorientation of the molecule, resulting in correlated spectral densities with respect to the diamagnetic relaxation. Cross-correlated relaxation between the Curie spin and the dipole–dipole interaction between two nuclear spins is a well-studied phenomenon [28,30–34]. It results in differential line broadening of the doublet components observed for two scalar-coupled nuclear spins.

To the best of our knowledge, the effects of cross-correlation between Curie and CSA relaxation have never been assessed. The present paper examines their relevance for determination of electron–nucleus distances by measurements of paramagnetic relaxation enhancements.

2. Theory

The evolution of the density matrix can be described by

$$\frac{\mathrm{d}}{\mathrm{d}t}\sigma_i = -\mathrm{i}\omega_i\sigma_i + \sum_j \Gamma_{i,j}(\sigma_j - \sigma_j^{\mathrm{eq}}), \tag{1}$$

where σ_i are the matrix elements of the density operator, σ_i^{eq} their corresponding equilibrium values and ω_i their oscillation frequencies [35]. The elements of the relaxation supermatrix $\Gamma_{i,j}$ are functions of the Hamiltonian terms H^μ responsible for relaxation, where μ identifies a particular relaxation mechanism. The elements of the relaxation supermatrix can readily be calculated when each of the Hamiltonian terms is decomposed into a sum of products, involving an interaction constant ξ_μ, a spin part (consisting of rank 2 irreducible spin tensor operators $T^\mu_{2,q}$), and a spatial part (usually the second-order spherical harmonics $Y^\mu_{2,q}$); this latter term reflects the time-dependent orientation $\Omega^\mu(t)$ of the principal axes of the interaction tensor [36]

$$H^\mu(t) = \xi_\mu \cdot \sum_{q=-2}^{+2} (-1)^q \cdot Y^\mu_{2,-q}(\Omega^\mu(t)) \cdot T^\mu_{2,q}. \tag{2}$$

The elements $\Gamma_{i,j}$ of the relaxation supermatrix can then be expressed as

$$\begin{aligned}\Gamma_{i,j} &= \sum_{\mu,\mu'} \Gamma^{\mu,\mu'}_{B_i,B_j} \\ &= \sum_{\mu,\mu'} \sum_q \frac{1}{2}\left\langle B_j \middle| \left[T^\mu_{2,-q}, \left[T^{\mu'}_{2,q}, B_i\right]\right]\right\rangle J^{\mu,\mu'}(\omega_q),\end{aligned} \tag{3}$$

where B_i are orthonormal basis spin operators of the Liouville space and $J^{\mu,\mu'}(\omega_q)$ are the spectral density functions of the molecular motions, defined as the real part of the Fourier transformed correlation function $\left\langle \xi_\mu \xi_{\mu'} Y^\mu_{2,0}(\Omega^\mu(t-\tau)) Y^{\mu'}_{2,0}(\Omega^{\mu'}(t))\right\rangle$

$$J^{\mu,\mu'}(\omega) = \mathrm{Re}\int_{-\infty}^{\infty} \mathrm{e}^{-\mathrm{i}\omega\tau}\left\langle \xi_\mu \xi_{\mu'} Y^\mu_{2,0}(\Omega^\mu(t-\tau)) Y^{\mu'}_{2,0}(\Omega^{\mu'}(t))\right\rangle \mathrm{d}\tau. \tag{4}$$

In the absence of contact interaction between nuclear and electronic spins, the most important components of the Hamiltonian H describing nuclear spin relaxation are due to dipole–dipole (DD) interactions between the nuclear spins, the Solomon (S) mechanism, chemical shielding anisotropy (CSA), and dipolar shielding anisotropy (DSA)

$$H = H^{\mathrm{DD}} + H^{\mathrm{S}} + H^{\mathrm{CSA}} + H^{\mathrm{DSA}}. \tag{5}$$

Table 1 presents explicit expressions for these terms in the situation, where a spin I is scalar coupled to a spin K (both nuclei with spin 1/2) and the I spin relaxes due to CSA (in the following assumed to be axially symmetric), nuclear dipole–dipole interactions and interac-

Table 1
Components of the Hamiltonian and relaxation rates describing the relaxation in a spin system composed of two nuclear spins 1/2 and and an electronic spin[a]

$H^{\mu} = \xi_{\mu}\sum_{q=-2}^{+2}(-1)^{q} Y^{\mu}_{2,-q} T^{\mu}_{2,q}$			Correlation time τ_c	*Auto-correlated* contributions to R_1 and R_2
μ	Interaction constant ξ_{μ}	Spin parts $T^{\mu}_{2,q}$		
DD [36]	$\xi_{DD} = -\sqrt{\frac{24\pi}{5}}\left(\frac{\mu_0}{4\pi}\right)\frac{\hbar\gamma_I\gamma_K}{r^3}$	$T_{2,0}(I,K) = \frac{1}{\sqrt{6}}[3I_zK_z - (I\cdot K)]$	$\tau_c = \tau_r$	$R_1^{DD} = \frac{1}{48\pi}\xi_{DD}^2\left(\frac{\tau_c}{1+(\omega_I-\omega_K)^2\tau_c^2} + \frac{3\tau_c}{1+\omega_I^2\tau_c^2} + \frac{6\tau_c}{1+(\omega_I+\omega_K)^2\tau_c^2}\right)$
		$T_{2,\pm1}(I,K) = \mp\frac{1}{2}[I_{\pm}K_z + I_zK_{\pm}]$		$R_2^{DD} = \frac{1}{96\pi}\xi_{DD}^2\left(4\tau_c + \frac{\tau_c}{1+(\omega_I-\omega_K)^2\tau_c^2} + \frac{3\tau_c}{1+\omega_I^2\tau_c^2} + \frac{6\tau_c}{1+\omega_K^2\tau_c^2} + \frac{6\tau_c}{1+(\omega_I+\omega_K)^2\tau_c^2}\right)$
		$T_{2,\pm2}(I,\mathrm{K}) = \frac{1}{2}I_{\pm}\mathrm{K}_{\pm}$		
S [22]	$\xi_S = -\sqrt{\frac{24\pi}{5}}\left(\frac{\mu_0}{4\pi}\right)\frac{\hbar\gamma_I\gamma_S}{r^3}$	$T_{2,0}(I,S) = \frac{1}{\sqrt{6}}[3I_zS_z - (I\cdot S)]$	$\frac{1}{\tau_c} = \frac{1}{\tau_e} + \frac{1}{\tau_r}$	$R_1^{S} = \frac{1}{48\pi}\xi_S^2\left(\frac{\tau_c}{1+(\omega_I-\omega_S)^2\tau_c^2} + \frac{3\tau_c}{1+\omega_I^2\tau_c^2} + \frac{6\tau_c}{1+(\omega_I+\omega_S)^2\tau_c^2}\right)$
		$T_{2,\pm1}(I,S) = \mp\frac{1}{2}[I_{\pm}S_z + I_zS_{\pm}]$		$R_2^{S} = \frac{1}{96\pi}\xi_S^2\left(4\tau_c + \frac{\tau_c}{1+(\omega_I-\omega_S)^2\tau_c^2} + \frac{3\tau_c}{1+\omega_I^2\tau_c^2} + \frac{6\tau_c}{1+\omega_S^2\tau_c^2} + \frac{6\tau_c}{1+(\omega_I+\omega_S)^2\tau_c^2}\right)$
		$T_{2,\pm2}(I,S) = \frac{1}{2}I_{\pm}S_{\pm}$		
CSA [36]	$\xi_{CSA} = \sqrt{\frac{8\pi}{15}}\gamma_I B_0 \Delta\sigma_I^{CSA}$	$T_{2,0}(I) = \frac{2}{\sqrt{6}}I_z$	$\tau_c = \tau_r$	$R_1^{CSA} = \frac{1}{4\pi}\xi_{CSA}^2\left(\frac{\tau_c}{1+(\omega_I\tau_c)^2}\right)$
				$R_2^{CSA} = \frac{1}{24\pi}\xi_{CSA}^2\left(4\tau_c + \frac{3\tau_c}{1+(\omega_I\tau_c)^2}\right)$
DSA [29]	$\xi_{DSA} = \sqrt{\frac{8\pi}{15}}\left(\frac{\mu_0}{4\pi}\right)\frac{\gamma_I B_0 \mu_B^2 g_e^2 S_e(S_e+1)}{r^3 kT} = \sqrt{\frac{8\pi}{15}}\gamma_I B_0 \Delta\sigma_I^{DSA}$	$T_{2,\pm1}(I) = \mp\frac{1}{2}I_{\pm}$		$R_1^{DSA} = \frac{1}{4\pi}\xi_{DSA}^2\left(\frac{\tau_c}{1+(\omega_I\tau_c)^2}\right)$
				$R_2^{DSA} = \frac{1}{24\pi}\xi_{DSA}^2\left(4\tau_c + \frac{3\cdot\tau_c}{1+(\omega_I\tau_c)^2}\right)$
ESA	$\xi_{ESA} = \sqrt{\xi_{CSA}^2 + \xi_{DSA}^2 + 2P_2(\cos\theta)\xi_{CSA}\xi_{DSA}}$	$T_{2,\pm2}(I) = 0$		$R_1^{ESA} = \frac{1}{4\pi}\xi_{ESA}^2\left(\frac{\tau_c}{1+(\omega_I\tau_c)^2}\right)$
				$R_2^{ESA} = \frac{1}{24\pi}\xi_{ESA}^2\left(4\tau_c + \frac{3\cdot\tau_c}{1+(\omega_I\tau_c)^2}\right)$

[a] The first column provides literature references for each mechanism. γ_I, γ_K, and γ_S are the magnetogyric ratios of the nuclear spins I and K and of the electronic spin S, respectively. ω_I, ω_K, and ω_S are their respective Larmor frequencies. τ_c, τ_r, and τ_e are the effective, the rotational, and the electronic correlation time, respectively. $\hbar$ is Planck's constant divided by 2π, μ_0 is the vacuum permeability, μ_B is the Bohr's magneton, B_0 is the magnetic field strength, k is the Boltzmann factor, T is the temperature, $\Delta\sigma_I^{CSA}$ and $\Delta\sigma_I^{DSA}$ are the anisotropies of the CSA and DSA tensors of the nucleus I; g_e and S_e are the electronic g-factor and spin; their values are replaced by g_J and J for lanthanides. r denotes the distance between spins I and K for the dipole–dipole mechanism, and the distance between spins I and S for the Solomon and DSA mechanisms.

tions with an electronic spin (assumed to be of isotropic magnetic susceptibility χ_{iso}), using the form of Eq. (2). The table clearly shows that the transformation properties of the Solomon effect are analogous to those of the DD effect. Furthermore, the relaxation contribution of the DSA is of a similar functional form as that of the CSA, if one defines the anisotropy of the dipolar shift tensor of a nucleus I [29] as

$$\Delta\sigma_I^{\mathrm{DSA}} = \frac{3\chi_{\mathrm{iso}}}{4\pi r^3} = \frac{\mu_{\mathrm{B}}^2 g_{\mathrm{e}}^2 S_{\mathrm{e}}(S_{\mathrm{e}}+1)}{r^3 kT}, \tag{6}$$

where μ_{B} is Bohr's magneton, k the Boltzmann factor, T the temperature, g_{e} and S_{e} are the electronic g-factor and spin number, respectively, and r is the distance between the nuclear and the electronic spin. In the case of lanthanides, g_{e} and S_{e} would be replaced by g_{j} and J, respectively. The DSA is the anisotropy of the rank 2 irreducible component σ_I^{DSA} of the dipolar shift tensor. $\Delta\sigma_I^{\mathrm{DSA}}$ denotes the DSA in the case of an axially symmetric σ_I^{DSA} tensor. $\Delta\sigma_I^{\mathrm{DSA}}$ is non-zero irrespective of the symmetry of the metal susceptibility χ. In the case of isotropic magnetic susceptibility, the spatial average of the dipolar shift tensor (the pseudocontact shift δ^{PCS}) vanishes and σ_I^{DSA} is axially symmetric. In the case of anisotropic magnetic susceptibility, δ^{PCS} is non-zero and σ_I^{DSA} non-axially symmetric [29].

The longitudinal and transverse relaxation rates R_1 and R_2 of the decoupled I spin are determined by the relaxation-supermatrix elements $\Gamma_{i,j} = \Gamma_{I_z,I_z}$ and $\Gamma_{i,j} = \Gamma_{I^+,I^+}$, respectively [35]. Calculation of these terms requires the evaluation of all possible auto ($\mu = \mu'$) and cross-products ($\mu \neq \mu'$) between the terms of the Hamiltonian in Eq. (5). As the correlation time of the Solomon relaxation mechanism is different from the correlation time characterizing the dynamics of the molecule, H^{S} does not correlate with the rest of the Hamiltonian. Cross-correlations between H^{DD} and H^{CSA} [37] and between H^{DD} and H^{DSA} [28] result in different relaxation rates for the doublet components of spin I, but they do not affect the auto-relaxation rates R_1 and R_2 of the I spin and can be eliminated by decoupling.

In contrast, H^{CSA} and H^{DSA} have identical spin parts and affect both lines of the I-spin doublet in the same way, so that cross-correlation between these two mechanisms contributes to the auto-relaxation rates similarly as $R_{1,2}^{\mathrm{DD}}$, $R_{1,2}^{\mathrm{S}}$, $R_{1,2}^{\mathrm{CSA}}$, and $R_{1,2}^{\mathrm{DSA}}$. This result is completely analogous to the situation of CSA relaxation, where the relaxation by a non-axially symmetric shielding tensor can be decomposed into the effects from two axially symmetric tensors and a cross-correlation term which affects both lines of a doublet equally [37]. In the case of isotropic molecular tumbling (described by a rotational correlation time τ_{r}) and axially symmetric CSA and DSA tensors, the corresponding spectral density is

$$J^{\mathrm{CSA}\times\mathrm{DSA}}(\omega) = \frac{1}{24\pi}\xi_{\mathrm{CSA}}\xi_{\mathrm{DSA}}P_2(\cos\theta^{\mathrm{CSA,DSA}})\left(\frac{\tau_{\mathrm{r}}}{1+(\omega\tau_{\mathrm{r}})^2}\right), \tag{7}$$

where P_2 is the second-order Legendre polynomial $[P_2(x) = (3x^2-1)/2]$ and $\theta^{\mathrm{CSA,DSA}}$ is the angle between the principal axes of the CSA and DSA tensors. The resulting effect on the longitudinal and transverse relaxation rates of the I spin is therefore:

$$R_1^{\mathrm{CSA}\times\mathrm{DSA}} = \frac{1}{4\pi}\left[2\xi_{\mathrm{CSA}}\xi_{\mathrm{DSA}}P_2(\cos\theta^{\mathrm{CSA,DSA}})\right]\left(\frac{\tau_{\mathrm{r}}}{1+(\omega_I\tau_{\mathrm{r}})^2}\right), \tag{8}$$

$$R_2^{\mathrm{CSA}\times\mathrm{DSA}} = \frac{1}{24\pi}\left[2\xi_{\mathrm{CSA}}\xi_{\mathrm{DSA}}P_2(\cos\theta^{\mathrm{CSA,DSA}})\right]\left(4\tau_{\mathrm{r}} + \frac{3\tau_{\mathrm{r}}}{1+(\omega_I\tau_{\mathrm{r}})^2}\right). \tag{9}$$

These terms share the functional form of the CSA and Curie-relaxation rates $R_{1,2}^{\mathrm{CSA}}$ and $R_{1,2}^{\mathrm{DSA}}$ (Table 1). Therefore, it is possible to combine the relaxation contributions by the CSA and DSA mechanisms into a new relaxation term governed by an effective shielding anisotropy (ESA) which is obtained by the sum of the CSA and DSA tensors (Fig. 1). The interaction constant of the ESA tensor resulting from the combination of the two tensors is

$$\xi_{\mathrm{ESA}} = \sqrt{\xi_{\mathrm{CSA}}^2 + \xi_{\mathrm{DSA}}^2 + 2P_2(\cos\theta^{\mathrm{CSA,DSA}})\xi_{\mathrm{CSA}}\xi_{\mathrm{DSA}}}. \tag{10}$$

The final expressions for the auto-relaxation rates become

$$\begin{aligned} R_{1,2} &= R_{1,2}^{\mathrm{DD}} + R_{1,2}^{\mathrm{S}} + R_{1,2}^{\mathrm{CSA}} + R_{1,2}^{\mathrm{DSA}} + R_{1,2}^{\mathrm{CSA}\times\mathrm{DSA}} \\ &= R_{1,2}^{\mathrm{DD}} + R_{1,2}^{\mathrm{S}} + R_{1,2}^{\mathrm{ESA}}, \end{aligned} \tag{11}$$

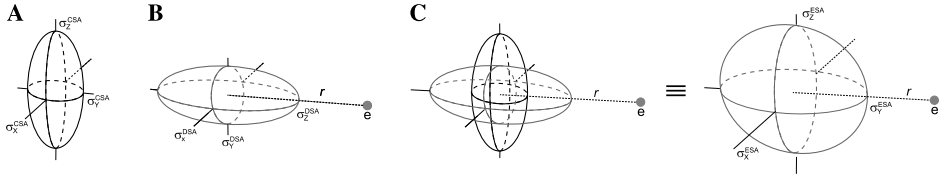

Fig. 1. Schematic representation of the shielding tensors involved in nuclear relaxation in an isotropically tumbling paramagnetic molecule. CSA (A) and DSA (B) tensors combine into an effective shielding anisotropy (ESA) tensor (C). For simplicity, the CSA and DSA tensors were assumed to be axially symmetric. e indicates the position of the paramagnetic center located at a distance r from the nuclear spin.

where

$$R_1^{\mathrm{ESA}} = R_1^{\mathrm{CSA}} + R_1^{\mathrm{DSA}} + R_1^{\mathrm{CSA\times DSA}} = \frac{1}{4\pi}\xi^2_{\mathrm{ESA}}\left(\frac{\tau_r}{1+(\omega_I\tau_r)^2}\right), \quad (12)$$

$$R_2^{\mathrm{ESA}} = R_2^{\mathrm{CSA}} + R_2^{\mathrm{DSA}} + R_2^{\mathrm{CSA\times DSA}} = \frac{1}{24\pi}\xi^2_{\mathrm{ESA}}\left(4\tau_r + \frac{3\tau_r}{1+(\omega_I\tau_r)^2}\right). \quad (13)$$

In the case of non-axially symmetric CSA or DSA, the relaxation rates can be calculated, in principle, in the same way, decomposing the anisotropic tensors into axially symmetric tensors and evaluating all pairwise interferences according to Eq. (7) [37].

3. Results and discussion

The contribution of the CSA×DSA cross-correlation rate $R_{1,2}^{\mathrm{CSA\times DSA}}$ to the R_1 and R_2 relaxation rates of a nuclear spin I depends on the distance r between the nuclear and electronic spin and on the relative orientation of the CSA and DSA tensors. In the case of axially symmetric CSA and DSA tensors

$$R_{1,2}^{\mathrm{CSA\times DSA}} \propto \xi_{\mathrm{CSA}}\cdot\xi_{\mathrm{DSA}}\cdot P_2(\cos\theta^{\mathrm{CSA,DSA}}) \propto \gamma_I^2 B_0^2 \Delta\sigma_I^{\mathrm{CSA}}\Delta\sigma_I^{\mathrm{DSA}}\cdot P_2(\cos\theta^{\mathrm{CSA,DSA}}) \propto \frac{P_2(\cos\theta^{\mathrm{CSA,DSA}})}{r^3}, \quad (14)$$

where γ_I is the magnetogyric ratio of nucleus I, B_0 is the magnetic field and $\Delta\sigma_I^{\mathrm{CSA}}$ and $\Delta\sigma_I^{\mathrm{DSA}}$ denote the anisotropies of the CSA and DSA tensors of nucleus I, respectively. This cross-correlation effect is proportional to the inverse of the third power of the nucleus–electron distance r_{eI} and modulated by the angle $\theta^{\mathrm{CSA,DSA}}$ between the principal axes of the CSA and DSA tensors. In the case of isotropic magnetic susceptibility, the principal axis of the DSA tensor coincides with the nucleus–electron vector.

Notably, the CSA×DSA cross-correlation effect is not eliminated by subtracting the contribution of the diamagnetic CSA from that of the effective shielding anisotropy (ESA) resulting from the superposition of CSA and DSA tensors. This has important implications for the measurement of distances between nuclear spins and paramagnetic centers, when the CSA of the nuclear spin and the DSA originating from the paramagnetic center are significant.

Paramagnetic relaxation enhancements are usually measured as the difference of the nuclear relaxation rate measured in the presence of the paramagnetic center and the corresponding relaxation rate measured for a diamagnetic reference. This procedure, however, yields

Table 2
Contributions of the Solomon (S) and Curie spin (DSA) mechanisms to paramagnetic nuclear relaxation in complexes with metal ions with different spin states S_e (J for lanthanides), g-factors, and electronic relaxation times τ_e for complexes of different rotational correlation time τ_r at different magnetic field strengths[a]

	$S_e(J)$	$g_e g_J$[b]	τ_e (10^{-13} s)[c]	$B_0 = 7$ T ($\omega_H/2\pi = 300$ MHz)					$B_0 = 14$ T ($\omega_H/2\pi = 600$ MHz)				
				R_1^S	R_1^{DSA}		R_2^S	R_2^{DSA}	R_1^S	R_1^{DSA}		R_2^S	R_2^{DSA}
					$\tau_r = 0.1$ ns	$\tau_r = 1$ ns		$\tau_r = 0.1$ ns		$\tau_r = 0.1$ ns	$\tau_r = 1$ ns		$\tau_r = 0.1$ ns	$\tau_r = 1$ ns
Fe^{3+}	1/2	2	5.0	6.3	0.1	0.03	6.4	0.1	4.5	0.4	0.03	4.7	0.5	32.5
	5/2	2	10.0	105	16.0	4.6	110	19.0	1110	72.7	58.1	4.7	80.6	73.3	4430
Ce^{3+}	5/2	6/7	1.33	4.4	0.5	0.2	4.4	0.6	37.4	4.2	2.0	0.2	4.2	2.5	149
Dy^{3+}	15/2	4/3	2.40	134	168	48.8	135	200	11600	116	610	49	118	770	46500
Yb^{3+}	7/2	8/7	1.57	16.4	5.5	1.6	16.4	6.6	380	15.3	20.1	1.6	15.4	25.3	1500

[a] All values of the longitudinal and transverse relaxation enhancements R_1 and R_2, respectively, are in s^{-1} and were calculated for a proton located 5 Å from the ion at 298 K and at magnetic field strengths of 7 and 14 T which correspond to ^{1}H NMR frequencies of 300 and 600 MHz, respectively.

[b] See p. 63 in [22].

[c] The values of τ_e assumed for Fe^{3+} correspond to average values reported for different myoglobins and cytochromes (see p. 84 in [22]); the τ_e values used for the lanthanides are those reported for their complexes with DTPA [38].

the sum of all auto-correlated paramagnetic relaxation rates and any contribution from CSA×DSA cross-correlation which is indistinguishable from the auto-correlated term.

Table 2 shows the relative contribution of the Solomon and Curie mechanisms to longitudinal and transverse nuclear relaxation rates, at different fields and molecular tumbling rates, for a selection of metal ions (low-spin and high-spin Fe^{3+}, Ce^{3+}, Yb^{3+}, and Dy^{3+}) with different isotropic susceptibilities χ_{iso} and electronic relaxation times τ_e. CSA×DSA cross-correlation can play a significant role only when the nuclear relaxation is driven predominantly by the interaction with the Curie spin rather than by the Solomon or other relaxation mechanisms. The effect is thus restricted to paramagnetic relaxation caused by unpaired electrons with fast electronic relaxation times. Its impact strongly depends on the molecular motional regime and is different for transverse and longitudinal magnetization [22,38].

3.1. Transverse relaxation

Fig. 2 shows how the contribution of CSA×DSA cross-correlation to transverse relaxation modulates the simple distance dependence which governs the Curie auto-correlated term

$$R_2^{\mathrm{DSA}} \propto \xi_{\mathrm{DSA}}^2 \propto \frac{1}{r^6}. \tag{15}$$

The calculations were performed for the case of Dy^{3+} which possesses the largest magnetic susceptibility among the paramagnetic ions used in NMR. Fig. 2A shows that the CSA×DSA cross-correlation effect alters the total paramagnetic relaxation enhancement R_2^{p} most significantly for $\theta = 0°$ and 90°, whereas R_2^{p} is identical to R_2^{DSA} for $\theta = 54.7°$ and 125.3°, as expected on the basis of Eq. (14). In the case of negative CSA, the sign of the CSA×DSA interference term is reversed, resulting in lesser relaxation enhancement for $\theta = 0°$ and increased relaxation enhancement for $\theta = 90°$.

In contrast to the Solomon mechanism, the Curie effect on transverse relaxation rates increases with increasing rotational correlation time. In the case of Dy^{3+}, transverse nuclear relaxation is predominantly enhanced by the Curie mechanism even at rotational correlation times as short as tens of picoseconds, whereas the Solomon mechanism plays a much lesser role (Fig. 2B, Table 2). The modulation arising from $R_2^{\mathrm{CSA\times DSA}}$ also increases with the rotational correlation time. To assess the practical importance of the effect, we assumed a chemical shielding anisotropy characteristic of amide protons ($\Delta\sigma^{\mathrm{CSA}} = 15$ ppm) [39]. Dashed and dotted lines in Fig. 2B indicate the maximum positive ($\theta^{\mathrm{CSA,\,DSA}} = 0°$) and negative ($\theta^{\mathrm{CSA,\,DSA}} = 90°$) correction due to the cross-correlation term relative to the situation of $R_2^{\mathrm{CSA\times DSA}} = 0$ obtained at $\theta^{\mathrm{CSA,\,DSA}} = 54.7°$. The results show that the relative contribution from the CSA×DSA cross-correlation effect may be neglected for small molecules, but it is important at increased rotational correlation times. For example, the relaxation enhancements observed in the range of 17–20 Å from the metal ion in a molecule with $\tau_r = 20$ ns can vary more than 3-fold, depending on the angle θ between the CSA and DSA tensors. At short distances from the metal ion, the cross-correlation effect becomes unimportant compared with the Curie auto-relaxation rate. At these short distances, however, ^{1}H NMR signals are broadened beyond detection. The distance range for which

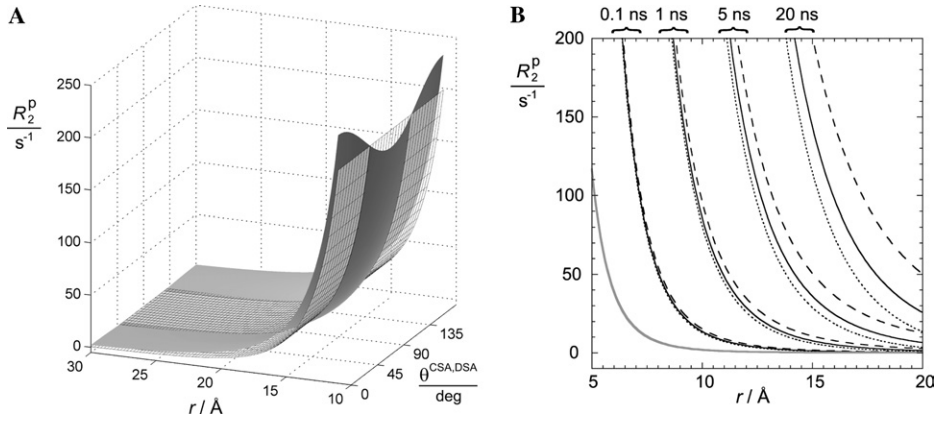

Fig. 2. Geometrical dependence of the paramagnetic contribution to transverse nuclear relaxation, R_2^{p}, in a molecule containing a Dy^{3+} ion. The paramagnetic relaxation-rate enhancement is plotted as a function of the proton-electron distance r and of the angle θ between the main axes of the CSA and DSA tensors, assuming axially symmetric CSA and DSA tensors and isotropic molecular tumbling. The simulations were performed for B_0=14 T, $T = 298$ K, and $\Delta\sigma_I^{\mathrm{CSA}} = 15$ ppm. (A) Total R_2^{p} (dark gray surface) for $\tau_c = 5$ ns compared with the contribution R_2^{DSA} from auto-correlated Curie relaxation alone (wire-frame surface). (B) Distance dependence of R_2^{p} plotted at θ values of 54.7° (solid line), 0° (dashed line), and 90° (dotted line), for different values of the rotational correlation time τ_r (0.1, 1, 5, and 20 ns). The contribution from the Solomon mechanism was calculated using $\tau_e = 2.40 \times 10^{13}$ s; it is therefore independent of the rotational correlation time for the motional regimes considered in the panel. The Solomon contribution is indicated by a gray solid line.

relaxation enhancements can readily be measured is also the range where the cross-correlation term is significant.

For most θ angles, the CSA×DSA cross-correlation effect enhances paramagnetically driven relaxation beyond the value predicted for Curie relaxation alone (Fig. 2B). The effect is particularly pronounced in the situation, where the CSA and DSA tensors are collinear (dashed lines in Figs. 2B and 3A). Interestingly, however, for certain other relative orientations of the CSA and DSA tensors, the CSA×DSA cross-correlation effect cannot only decrease the paramagnetic relaxation enhancement, but even result in line widths narrower than for the diamagnetic reference. This "paramagnetically effected narrowing" (PEN) effect occurs when both tensors are orthogonal with respect to each other $[P_2(\cos\theta^{\mathrm{CSA,\,DSA}}) < 0]$ and $|R_2^{\mathrm{CSA\times DSA}}| > |R_2^{\mathrm{DSA}} + R_2^{\mathrm{SB}}|$. The CSA×DSA cross-correlation can dominate over the auto-correlated Curie contribution at longer distances due to its lesser distance dependence (Table 1). In principle, the PEN effect exists at any rotational correlation time, but is in practice restricted to macromolecules, since long proton–electron distances are required (Fig. 3A). It requires that the main axes of the CSA and DSA tensors deviate from orthogonality by no more than about ±33° (Fig. 3B). For the values of $\Delta\sigma^{\mathrm{CSA}}$ and $\Delta\sigma^{\mathrm{DSA}}$ chosen in the example of Fig. 3, it requires a proton–electron distance r greater than 26 Å and is predicted to be maximum for $\theta^{\mathrm{CSA,DSA}} = 90°$ and $r = 32.4$ Å. Even at this optimum, the effect is small ($R_2^{\mathrm{p}} = -1.4\ \mathrm{s}^{-1}$, corresponding to line narrowing by about 0.5 Hz) and would be difficult to observe experimentally for a molecule with a rotational correlation time as assumed in the calculation (20 ns). It may, however, be more significant for spins for which CSA relaxation is the predominant relaxation mechanism in the diamagnetic state. In physical terms, the PEN effect can be understood as a mutual compensation of the anisotropies of chemical shielding (CSA) and dipolar shielding (DSA), see Fig. 1.

The PEN effect described here is fundamentally different from the previously reported "paramagnetic induced narrowing" (PIN) effect [31] which arises from the cross-correlation effect between the Curie spin and nuclear dipolar coupling. Whereas the PIN effect is active only for single doublet components, the PEN effect applies to every component of a multiplet as well as to singlets arising from isolated spins.

The CSA×DSA cross-correlation effect has important consequences for the extraction of distance restraints from paramagnetic relaxation enhancements. Usually, R_2^{p} values are converted into distance constraints r^{calc} using the relationship

$$r^{\mathrm{calc}} = \frac{k}{\sqrt[6]{R_2^{\mathrm{p}}}} \tag{16}$$

after a calibration procedure to determine the value of the scaling factor k. Without knowledge of the three-dimensional structure and the shape and orientation of the CSA and DSA tensors, the CSA×DSA cross-correlation effect cannot be taken into account.

Fig. 4 shows that the CSA×DSA cross-correlation effect substantially increases the uncertainty of distance measurement for longer distances for a molecule containing a Dy^{3+} ion. The range of rotational correlation times assumed in the example ($\tau_r = 5$ and 20 ns) encompasses most biological macromolecules studied by high-resolution NMR spectroscopy. It is instructive to compare the uncertainty generated by the lack of knowledge of the CSA×DSA cross-correlation contribution to the overall paramagnetic relaxation enhancement (dashed and dotted lines in Fig. 4) with the error introduced by a distance-independent uncertainty in the relaxation-rate measurement of about $3\ \mathrm{s}^{-1}$ which corresponds to an uncertainty of 1 Hz in line-width measurements (shaded areas in Fig. 4). In both cases, the uncertainties increase with increasing proton–electron distance, where the paramagnetic relaxation enhancement is less pronounced. The uncertainty introduced by the CSA×DSA cross-correla-

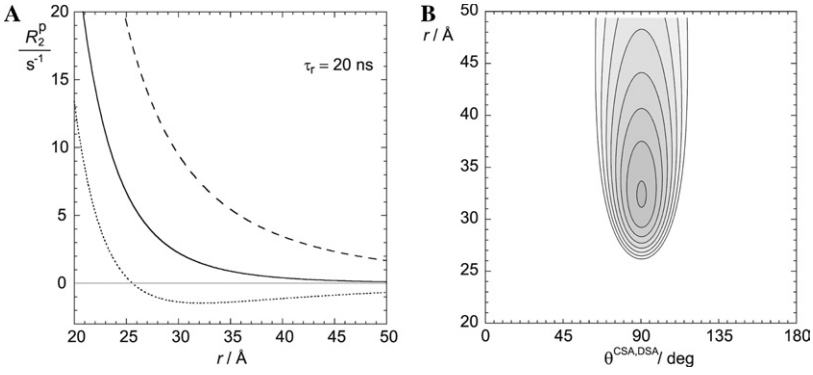

Fig. 3. Paramagnetically effected narrowing (PEN) of ^{1}H NMR resonances due to CSA×DSA cross-correlation. The paramagnetic relaxation enhancement R_2^{p} is shown for the distance range of 20–50 Å in a molecule containing a Dy^{3+} ion, assuming $\tau_r = 20$ ns. The same parameters were used in the simulation as in Fig. 2. (A) The curves were calculated for $\theta = 54.7°$ (solid line), 0° (dashed line), and 90° (dotted line). (B) Contours corresponding to negative values of R_2^{p}. The range of negative R_2^{p} values is identified by shading, with the lowest contour line at $-1.4\ \mathrm{s}^{-1}$.

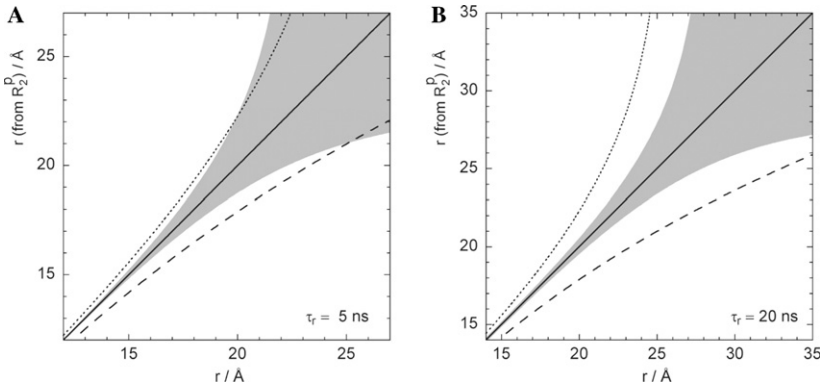

Fig. 4. Correlations between metal–proton distances r (horizontal axes) and corresponding values back-calculated from transverse relaxation data (vertical axes) simulated for a Dy^{3+} complex using Eq. (15). The plots refer to complexes with rotational correlation times $\tau_r = 5$ (A) and 20 ns (B). The R_2^p values were predicted using Eq. (12), assuming axially symmetric tensors with angles θ of 54.7° (solid line), 0° (dashed line), and 90° (dotted line) between the principal axes. The deviations from linearity introduced by CSA×DSA cross-correlation can be compared with the uncertainty caused by an experimental error of about 3 s^{-1} in R_2^p (shaded areas), corresponding to an uncertainty in line-width measurement of 1 Hz. The distance range displayed corresponds to R_2^p values in the range of 200–1 s^{-1}.

tion effect is particularly detrimental at shorter proton–electron distances. In the case of $\tau_r = 20$ ns and for distances in the range between 20 and 25 Å (Fig. 4B), the uncertainty caused by the cross-correlation is about 10-fold larger than that associated with an experimental error of 3 s^{-1} in R_2^p measurements. This fact must be taken into account whenever paramagnetic ions are used to derive long-range distance restraints in structure determinations of proteins or other biological macromolecules.

Curie and Solomon mechanisms contribute differently to the overall paramagnetic relaxation enhancements for metal ions with different electronic relaxation time, electronic spin and g-factor (Table 2). Fig. 5 illustrates the CSA×DSA cross-correlation effect for the metal ions and spin-states listed in Table 2 other than Dy^{3+}. The rotational correlation time was assumed to be 5 ns. The metal ions were sorted by decreasing Solomon contribution to the overall paramagnetic relaxation enhancement observed on a proton spin. The series shows that an increased weight of the Solomon mechanism improves the accuracy of distance measurement, as this decreases the impact of the CSA×DSA cross-correlation effect.

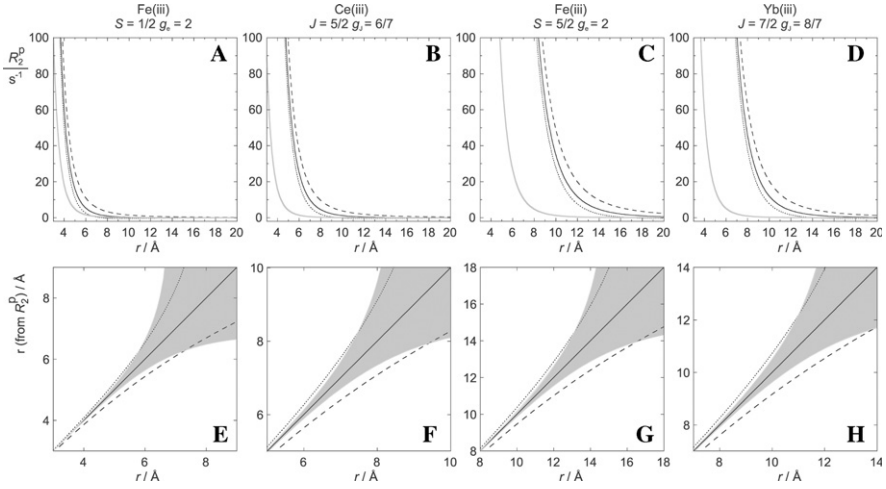

Fig. 5. Nuclear paramagnetic relaxation rate enhancements and back-calculated ^{1}H–metal distances as a function of real ^{1}H–metal distances in complexes with (A and E) low-spin Fe^{3+}, (B and F) Ce^{3+}, (C and G) high-spin Fe^{3+}, and (D and H) Yb^{3+}. (A–D) The transverse relaxation rate enhancements R_2^p were calculated separately for the parts associated with Curie-spin and Solomon mechanisms. Broad gray lines identify the contribution from the Solomon mechanism, while the contribution originating from the Curie spin is plotted for $\theta = 54.7°$ (solid line), 0° (dashed line), and 90° (dotted line). Other parameters used were $\tau_c = 5$ ns, $B_0 = 14$ T, and $T = 298$ K. Electronic relaxation times of Table 2 were used for the respective four ions. (E–H) Correlation between the back-calculated ^{1}H–metal distances (using Eq. (15)) and the real distances used to calculate the R_2^p values (using the formula of Table 1). Solomon and Curie auto-correlation terms were included in the calculation of the transverse nuclear relaxation enhancements R_2^p together with the cross-correlated CSA×DSA contribution. Calculations were performed for$\theta = 54.7°$ (solid line), 0° (dashed line), and 90° (dotted line). The distance range displayed for each ion corresponds to R_2^p values between 200 and 1 s^{-1}. As in Fig. 3, shaded areas outline the uncertainty in distance determination arising from an experimental error in the determination of the R_2^p relaxation rates of 1 s^{-1}.

3.2. Longitudinal relaxation

Whereas a paramagnetic center in a macromolecule often broadens the NMR resonances near the paramagnetic metal ion beyond detection, rapidly tumbling small molecules experience lesser paramagnetic line broadening. Paramagnetic enhancements of longitudinal magnetization can thus readily be measured also for small molecules [40,41] and the influence from CSA×DSA cross-correlation effects on distance measurements can be significant in practical applications [42].

In contrast to transverse relaxation, longitudinal relaxation enhancement by Curie-spin relaxation depends on the spectral density at the nuclear frequency, but not the spectral density at zero frequency. As a consequence, the R_1^{DSA} enhancement is predicted to increase with increasing rotational correlation times τ_r to a maximum at $\tau_r = 0.3$ ns (for a ^{1}H Larmor frequency of 600 MHz), decreasing again with longer correlation times. The Curie relaxation enhancement can thus exceed the Solomon contribution only for small molecules, with typical τ_r values ranging from 0.1 to 1 ns, which are complexed to metal ions with large magnetic susceptibilities. Among the metal ions listed in Table 2, these conditions are readily satisfied in the case of Dy^{3+} (Fig. 6A–C), but not for the other ions (Fig. 6D–K). The angular dependence of the longitudinal relaxation enhancement due to DSAxCSA cross-correlation is

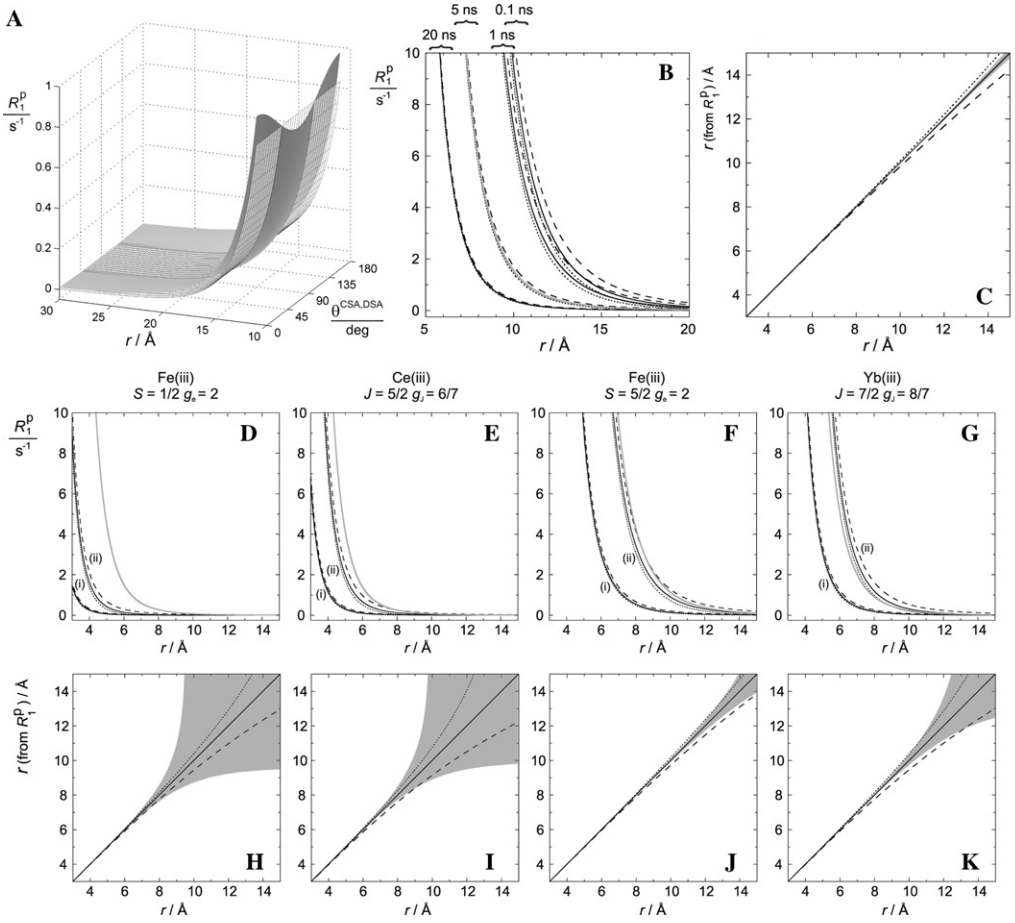

Fig. 6. Geometrical dependence of the paramagnetic contributions to nuclear longitudinal relaxation in a molecule containing Dy^{3+}, Fe^{3+} (low and high spin), Ce^{3+}, and Yb^{3+}. The paramagnetic terms are shown as a function of the proton–electron distance r and of the angle θ between the principal axes of the CSA and DSA tensors, assuming axially symmetric CSA and DSA tensors and an isotropically tumbling molecule. (A) Total R_1^p (dark gray surface) compared with the contribution R_1^{DSA} from auto-correlated Curie relaxation alone (wire-frame surface). Other parameters used for the simulation were $B_0 = 14$ T, $T = 298$ K, and $\Delta\sigma_J^{CSA} = 15$ ppm. (B and D–G) Distance dependence of R_1^p for the case of Dy^{3+} (B), low-spin Fe^{3+} (B), Ce^{3+} (E), high-spin Fe^{3+} (F), and Yb^{3+} (G) complexes, plotted for $\theta = 54.7°$ (solid line), 0° (dashed line), and 90° (dotted line). (B) The results for different values of the rotational correlation time τ_r (0.1, 1, 5, 10, and 20 ns); (D–G) for $\tau_r = 5$ ns (i) and $\tau_r = 0.1$ ns (ii). The relaxation enhancements associated with the Curie-spin and Solomon mechanisms were calculated separately. The contribution of the Solomon mechanism is shown by broad gray lines. The electronic relaxation times of Table 2 were used for the five ions. (C and H–K) Back-calculated ^{1}H–metal distances as a function of real ^{1}H–metal distances in complexes with (C) Dy^{3+}, (H) low-spin Fe^{3+}, (I) Ce^{3+}, (J) high-spin Fe^{3+}, and (K) Yb^{3+}. The curves were calculated for $\theta = 54.7°$ (solid line), 0° (dashed line), and 90° (dotted line), and refer to complexes with a rotational correlation times $\tau_r = 0.1$ ns. Other parameters used were $B_0 = 14$ T and $T = 298$ K. Shaded areas outline the uncertainty in distance determination arising from an experimental error in the determination of the R_1^p relaxation rates of 0.1 s^{-1}.

similar to that of transverse relaxation (Fig. 6A), but the paramagnetic enhancements R_1^{DSA} are much smaller compared with the corresponding R_2^{DSA} values. The corrections due to the $R_1^{DSAxCSA}$ term are also much smaller (Fig. 6B) and appreciable only in the fast-tumbling regime. Even then, the cross-correlation effect will hardly affect distance measurements, since molecules with short correlation times are usually not sufficiently big to afford ^{1}H–electron distances longer than 10 Å (Fig. 6C). For the other metal ions of Table 2, distances derived from measurements of paramagnetically enhanced longitudinal relaxation are similarly insensitive to the cross-correlation term, with errors resulting predominantly from experimental uncertainties.

4. Conclusions

Metal ions with fast relaxing electronic spins and large, anisotropic susceptibilities present a rich source of long-range structural restraints, including distance and angular information. Anisotropic susceptibility tensors are a prerequisite for the observation of pseudocontact shifts and molecular paramagnetic alignment in the magnetic field. In addition, the average susceptibility enhances the relaxation rates of the nuclear spins in a distance-dependent fashion, providing a relaxation mechanism which is also the source of cross-correlation effects with nuclear dipole–dipole relaxation and other relaxation mechanisms. Paramagnetic relaxation enhancements present a most obvious manifestation of paramagnetism and are commonly assumed to follow a $1/r^6$ distance dependence.

The present simulations show that the presence of CSA×DSA cross-correlation leads to a far more complicated situation. The effect provides an explanation, why simple subtraction of the relaxation rates of a diamagnetic reference from the experimental paramagnetic values often results in inaccurate distance measurements [43–45]: this procedure can only compensate for the auto-correlated CSA contribution. The cross-correlation effect can be of significant magnitude and may, under certain circumstances, even result in NMR signals which are narrower than in the diamagnetic protein. Clearly, this would seriously compromise the extraction of distances from paramagnetic relaxation rate enhancements.

The cross-correlation effect influences in particular the transverse relaxation rates in slowly tumbling macromolecules and, to a lesser extent, the longitudinal relaxation rates of rapidly tumbling molecules, when the molecules contain metal ions with high paramagnetic susceptibility. In contrast, transverse relaxation rates in small molecules and longitudinal relaxation rates in macromolecules are less affected due to a more predominant Solomon contribution, resulting in a purer $1/r^6$ distance dependence of the paramagnetic relaxation enhancement. The problem is confounded by the fact that auto-correlated DSA and cross-correlated CSA–DSA effects cannot be separated experimentally.

Quite generally, the effect only occurs, when the nuclear relaxation enhancements are predominantly driven by Curie relaxation, i.e., for metal ions with rapidly relaxing electronic spins (e.g., Ce^{3+}, Fe^{3+}, Yb^{3+}, Dy^{3+}) but not paramagnetic centers with slowly relaxing electronic spins (e.g., Mn^{2+}, Gd^{3+}, nitroxide radicals). Clearly, the latter ions are more universally applicable reagents for distance measurements from paramagnetic enhancements.

Acknowledgments

We thank Prof. Jozef Kowalewski for valuable discussions and for a critical reading of the manuscript. G.P. thanks the EU for a postdoctoral fellowship within the Research Training Network on Cross-Correlation (HPRN-CT-2000-00092). G.O. thanks the Australian Research Council for a Federation Fellowship. Financial support by the Australian Research Council is gratefully acknowledged.

References

[1] L. Banci, I. Bertini, C. Luchinat, Nuclear and Electron Relaxation: The Magnetic Nucleus-Unpaired Electron Coupling in Solution, VCH, Weinheim, 1991.
[2] I. Bertini, C. Luchinat, G. Parigi, Paramagnetic constraints: an aid for quick solution structure determination of paramagnetic metalloproteins, Concept Magn. Reson. 14 (2002) 259–286.
[3] L. Banci, I. Bertini, G. Cavallaro, A. Giachetti, C. Luchinat, G. Parigi, Paramagnetism-based restraints for Xplor-NIH, J. Biomol. NMR 28 (2004) 249–261.
[4] J.L. Battiste, G. Wagner, Utilization of site-directed spin labeling and high-resolution heteronuclear nuclear magnetic resonance for global fold determination of large proteins with limited nuclear Overhauser effect data, Biochemistry 39 (2000) 5355–5365.
[5] M. Ubbink, M. Ejdebäck, B.G. Karlsson, D.S. Bendall, The structure of the complex of plastocyanin and cytochrome *f*, determined by paramagnetic NMR and restrained rigid-body molecular dynamics, Structure 6 (1998) 323–335.
[6] A. Ramos, G. Varani, A new method to detect long-range protein–RNA contacts: NMR detection of electron–proton relaxation induced by nitroxide spin-labeled RNA, J. Am. Chem. Soc. 120 (1998) 10992–10993.
[7] J. Iwahara, D.E. Anderson, E.C. Murphy, G.M. Clore, EDTA-derivatized deoxythymidine as a tool for rapid determination of protein binding polarity to DNA by intermolecular paramagnetic relaxation enhancement, J. Am. Chem. Soc. 125 (2003) 6634–6635.
[8] T.K. Mal, M. Ikura, L.E. Kay, The ATCUN domain as a probe of intermolecular interactions: application to calmodulin–peptide complexes, J. Am. Chem. Soc. 124 (2002) 14002–14003.
[9] M.N. Harris, C.M. Bertolucci, L.J. Ming, Paramagnetic cobalt(II) as a probe for kinetic and NMR relaxation studies of phosphate binding and the catalytic mechanism of Streptomyces dinuclear aminopeptidase, Inorg. Chem. 41 (2002) 5582–5588.

[10] M. Gochin, A high-resolution structure of a DNA-chromomycin-Co(II) complex determined from pseudocontact shifts in nuclear magnetic resonance, Struct. Fold Des. 8 (2000) 441–452.
[11] W. Jahnke, S. Rudisser, M. Zurini, Spin label enhanced NMR screening, J. Am. Chem. Soc. 123 (2001) 3149–3150.
[12] J.D. Epperson, L.J. Ming, Proton NMR studies of Co(II) complexes of the peptide antibiotic bacitracin and analogues: insight into structure–activity relationship, Biochemistry 39 (2000) 4037–4045.
[13] X. Wei, L.J. Ming, Comprehensive 2D ^{1}H NMR studies of paramagnetic lanthanide(III) complexes of anthracycline antitumor antibiotics, Inorg. Chem. 37 (1998) 2255–2262.
[14] L.J. Ming, J.D. Epperson, Metal binding and structure–activity relationship of the metalloantibiotic peptide bacitracin, J. Inorg. Biochem. 91 (2002) 46–58.
[15] S. Kobayashi, Lanthanides: Chemistry and Use in Organic Synthesis, Springer, New York; London, 1999.
[16] L. Di Bari, M. Lelli, G. Pintacuda, G. Pescitelli, F. Marchetti, P. Salvadori, Solution versus solid-state structure of ytterbium heterobimetallic catalysts, J. Am. Chem. Soc. 125 (2003) 5549–5558.
[17] M. Shibasaki, N. Yoshikawa, Lanthanide complexes in multifunctional asymmetric catalysis, Chem. Rev. 102 (2002) 2187–2209.
[18] F.H. Allain, G. Varani, Divalent metal ion binding to a conserved wobble pair defining the upstream site of cleavage of group I self-splicing introns, Nucleic Acids Res. 23 (1995) 341–350.
[19] L. Di Bari, G. Pintacuda, S. Ripoli, P. Salvadori, Structure of metal adducts of anthracyclines probed by absorption, circular dichroism and paramagnetic NMR, Magn. Reson. Chem. 40 (2002) 396–405.
[20] R.L. Gonzalez Jr., I. Tinoco Jr., Identification and characterization of metal ion binding sites in RNA, Methods Enzymol. 338 (2001) 421–443.
[21] I. Bertini, Y.M. Lee, C. Luchinat, M. Piccioli, L. Poggi, Locating the metal ion in calcium-binding proteins by using cerium(III) as a probe, Chembiochem 2 (2001) 550–558.
[22] I. Bertini, C. Luchinat, G. Parigi, Solution NMR of Paramagnetic Molecules: Applications to Metallobiomolecules and Models, Elsevier, Amsterdam; London, 2001.
[23] I. Solomon, Relaxation processes in a system of two spins, Phys. Rev. 99 (1955) 559–565.
[24] L. Bertini, C. Luchinat, G. Parigi, Magnetic susceptibility in paramagnetic NMR, Prog. NMR Spectrosc. 40 (2002) 249–273.
[25] M. Guéron, Nuclear relaxation in macromolecules by paramagnetic ions: a novel mechanism, J. Magn. Reson. 19 (1975) 58–66.
[26] A.J. Vega, D. Fiat, Nuclear relaxation processes of paramagnetic complexes. The slow motion case, Mol. Phys. 31 (1976) 347–355.
[27] I. Bertini, C. Luchinat, D. Tarchi, Are true scalar proton proton connectivities ever measured in cosy spectra of paramagnetic macromolecules?, Chem. Phys. Lett. 203 (1993) 445–449.
[28] R. Ghose, J.H. Prestegard, Electron spin-nuclear spin cross-correlation effects on multiplet splittings in paramagnetic proteins, J. Magn. Reson. 128 (1997) 138–143.
[29] I. Bertini, J. Kowalewski, C. Luchinat, G. Parigi, Cross correlation between the dipole–dipole interaction and the Curie spin relaxation: the effect of anisotropic magnetic susceptibility, J. Magn. Reson. 152 (2001) 103–108.
[30] J. Boisbouvier, P. Gans, M. Blackledge, B. Brutscher, D. Marion, Long-range structural information in NMR studies of paramagnetic molecules from electron spin-nuclear spin cross-correlated relaxation, J. Am. Chem. Soc. 121 (1999) 7700–7701.
[31] P.K. Madhu, R. Grandori, K. Hohenthanner, P.K. Mandal, N. Müller, Geometry dependent two-dimensional heteronuclear multiplet effects in paramagnetic proteins, J. Biomol. NMR 20 (2001) 31–37.
[32] G. Pintacuda, K. Hohenthanner, G. Otting, N. Müller, Angular dependence of dipole–dipole-Curie-spin cross-correlation effects in high-spin and low-spin paramagnetic myoglobin, J. Biomol. NMR 27 (2003) 115–132.
[33] I. Bertini, G. Cavallaro, M. Cosenza, R. Kummerle, C. Luchinat, M. Piccioli, L. Poggi, Cross correlation rates between Curie spin and dipole–dipole relaxation in paramagnetic proteins: the case of cerium substituted calbindin D9k, J. Biomol. NMR 23 (2002) 115–125.
[34] F. Kateb, M. Piccioli, New routes to the detection of relaxation allowed coherence transfer in paramagnetic molecules, J. Am. Chem. Soc. 125 (2003) 14978–14979.
[35] R.R. Ernst, G. Bodenhausen, A. Wokaun, Principles of Nuclear Magnetic Resonance in One and Two Dimensions, Clarendon Press, Oxford, 1987.
[36] A. Abragam, Principles of Nuclear Magnetism, Clarendon Press, Oxford, 1986.
[37] M. Goldman, Interference effects in the relaxation of a pair of unlike spin-1/2 nuclei, J. Magn. Reson. 60 (1984) 437–452.
[38] B.M. Alsaadi, F.J.C. Rossotti, R.J.P. Williams, Hydration of complexone. Complexes of lanthanide cations, J. Chem. Soc. Dalton (1980) 2151–2154.
[39] G. Cornilescu, A. Bax, Measurement of proton, nitrogen, and carbonyl chemical shielding anisotropies in a protein dissolved in a dilute liquid crystalline phase, J. Am. Chem. Soc. 122 (2000) 10143–10154.
[40] S. Aime, M. Botta, G. Ermondi, NMR-study of solution structures and dynamics of lanthanide(III) complexes of DOTA, Inorg. Chem. 31 (1992) 4291–4299.
[41] S. Aime, L. Barbero, M. Botta, G. Ermondi, Determination of metal proton distances and electronic relaxation-times in lanthanide complexes by nuclear-magnetic-resonance spectroscopy, J. Chem. Soc. Dalton (1992) 225–228.
[42] J.A. Peters, J. Huskens, D.J. Raber, Lanthanide induced shifts and relaxation rate enhancements, Prog. NMR Spectrosc. 28 (1996) 283–350.
[43] M. Gochin, Nuclear magnetic resonance characterization of a paramagnetic DNA-drug complex with high spin cobalt; assignment of the ^{1}H and ^{31}P NMR spectra, and determination of electronic, spectroscopic and molecular properties, J. Biomol. NMR 12 (1998) 243–257.
[44] M.D. Kemple, B.D. Ray, K.B. Lipkowitz, F.G. Prendergast, B.D.N. Rao, The use of lanthanides for solution structure determination of biomolecules by NMR—Evaluation of the methodology with EDTA derivatives as model systems, J. Am. Chem. Soc. 110 (1988) 8275–8287.
[45] G. Pintacuda, M.A. Keniry, T. Huber, A.Y. Park, N.E. Dixon, G. Otting, Fast structure-based assignment of ^{15}N HSQC spectra of selectively ^{15}N-labeled paramagnetic proteins, J. Am. Chem. Soc. 126 (2004) 2963–2970.